Urban anomalies in response to rainstorms based on smartphone location data: a case study of eight cities in China

Jiawei Yi[1,2], Yunyan Du[1,2*], Fuyuan Liang[3], Tao Pei[1,2], Ting Ma[1,2], Chenghu Zhou[1,2]

[1]State Key Laboratory of Resources and Environmental Information System, Institute of Geographic Science and Natural Resources Research, Chinese Academy of Sciences, Beijing, China

[2]University of Chinese Academy of Sciences, Beijing, China

[3]Department of Geography, Western Illinois University, Macomb, IL, USA

*Corresponding author: duyy@lreis.ac.cn

Abstract

This study explored city residents' collective geo-tagged behaviors in response to rainstorms using the number of location request (NLR) data generated by smartphone users. We examined the rainstorms, flooding, NLR anomalies, as well as the associations among them in eight selected cities across the mainland China. The time series NLR clearly reflects cities' general diurnal rhythm and the total NLR is moderately correlated with the total city population. Anomalies of NLR were identified at both the city and grid scale using the S-H-ESD method. Analysis results manifested that the NLR anomalies at the city and grid levels are well associated with rainstorms, indicating city residents request more location-based services (e.g. map navigation, car hailing, food delivery, etc.) when there is a rainstorm. However, sensitivity of the city residents' collective geo-tagged behaviors in response to rainstorms varies in different cities as shown by different peak rainfall intensity thresholds. Significant high peak rainfall intensity tends to trigger city flooding, which lead to increased location-based requests as shown by positive anomalies on the time series NLR.

Keywords: urban anomaly; rainstorm disaster; human response; rainfall intensity threshold; anomaly score

1 Introduction

Global climate change is making rainfall events heavier and more frequent in many areas. Powerful rainstorms may flood a city once the rainfall exceeds the discharge capacity of a city's drainage system. Inundation of cities' critical infrastructures and populated communities tends to disrupt urban residents' social and economic activities and even cause dramatic life and property losses (Papagiannaki et al. 2013; Spitalar et al. 2014; Liao et al. 2019). Floods nowadays are the most common type of natural disaster, which poses a serious threat to the safety of life and property in most countries (Alexander et al. 2006; Min et al. 2011; Hu et al. 2018). According to the released survey in the Bulletin of Flood and Drought

Disasters in China, more than 104 cities were struck by floods in 2017, affecting up to 2.18 million population and causing over 2.46 billion US dollars direct economic losses (China National Climate Center 2017).

The impacts of a rainstorm are usually evaluated with respect to the interactions among rainfall intensity, the population exposure, the urban vulnerability, and the society coping capacity (Spitalar et al. 2014; Papagiannaki et al. 2017). The rainfall intensity that may trigger flood disasters has been extensively investigated and many studies have examined the relationship between rainfall intensities and social responses (Ruin et al. 2014; Papagiannaki et al. 2015; Papagiannaki et al. 2017). Nowadays the peak rainfall intensity is widely used to determine the critical rainfall threshold for issuing flash flood warnings (Cannon et al. 2007; Diakakis 2012; Miao et al. 2016).

The population exposure refers to the spatial domain of population and properties that would be affected by a rainfall hazard (Ruin et al. 2008). Gradual increase in the proportion of population living in urban areas due to urbanization makes more people exposed and vulnerable to urban flash floods, posing great challenge to flood risk reduction (Liao et al. 2019). Reduction of vulnerability therefore becomes critical in urban disaster mitigation. Vulnerability is usually assessed by comprehensively considering related physical, social, and environmental factors (Kubal et al. 2009; Adelekan 2011; Zhou et al. 2019), and their dynamic characteristics across space and time (Terti et al. 2015).

Coping capacity reflects the ability of a society to handle adverse disaster conditions and it is one of the most important things to consider in disaster mitigation (UNISDR 2015). The coping capacity is usually evaluated by examining the human behaviors in response to disasters, which are mainly collected by post-disaster field investigation and questionnaires (Taylor et al. 2015). Such conventional approaches only provide limited samples that may not be able to fully and timely reflect disaster-induced human behaviors. Recently, researchers have learned the advantages of using unconventional data sets such as insurance claims (Barberia et al. 2014), newspapers (Llasat et al. 2009), and emergency operations and calls (Papagiannaki et al. 2015; Papagiannaki et al. 2017) to quantify the coping capacity.

The growing use of smartphones and location-based services (LBS) in recent years has generated massive geospatial data, which could be used to infer the collective geo-tagged human activities. The geospatial data thus provides a new perspective to study normal urban rhythm in regular days (Ratti et al. 2006; Ma et al. 2019) and abnormal human behaviors in response to emergencies (Goodchild & Glennon 2010; Wang & Taylor 2014; Kryvasheyeu et al. 2016). Bagrow et al. (2011)

found the number of phone calls spiked during earthquake, blackout, and storm emergencies. Dobra et al. (2015) explored the spatiotemporal variations in the anomaly patterns caused by different emergencies. Gundogdu et al. (2016) reported that it is possible to identify the anomalies inflicted by emergencies or non-emergency events from mobile phone data using a stochastic method. In addition to the afore-mentioned applications, more studies are needed to explore the full potential of the mobile phone data in terms of revealing human collective behaviors, particularly in response to hazards and emergencies.

This study explored the urban anomalies and their variations in response to rainstorms using the NLR requests from smartphone users. We selected eight representative cities in the mainland China to examine how urban residents response to typical summer rainstorms in different regions. The anomalies of LBS requests caused by rainstorms were identified using a time series decomposition method and then described by multiple indices, which are used to study how rainstorms affect geo-tagged human behaviors collectively. The rest of the paper is organized as follows. Section 2 introduces the selected cities and the smartphone NLR dataset. Section 3 presents the anomaly detection and description methods. Section 4 provides the analysis results including rainfall statistics, normal rhythms, and rainstorm-triggered anomalies in the selected cities. Section 5 concludes the study and discusses the future work.

2 Materials

2.1 Study area

We selected eight representative cities across the mainland China for this study (Fig. 1). Two cities were selected from each region except the northwestern and southwestern China (Table 1). The eight cities vary significantly with respect to their total population, footprint areas, and urbanization rate. In this study, the footprint of a city is composed of the grids that have an hourly number of location requests (NLR) no less than the median of the daily NLR time series of that grid over the whole month, i.e., the grids with at least one NLR every hour in average.

Haikou and Zhuhai are located in southern China which has mean annual precipitation between 1600 mm and 3000 mm. Among the eight cities, Zhuhai is the least populated city but with the highest urbanization rate. In central China, we selected Hefei and Xiangyang, which have mean annual precipitation between 800 mm and 1600 mm. Two cities, Lanzhou and Hengshui, were selected from a semi-humid region in northern China with mean annual precipitation between 400 mm and 800 mm. Hengshui has the largest footprint area but the least urbanization

rate among the cities. Harbin and Jilin are located in the Northeastern China. The mean annual precipitation of Harbin and Jilin ranges from 400 mm to 800 mm and between 800 mm and 1600 mm, respectively. Harbin is the most populated among the eight cities.
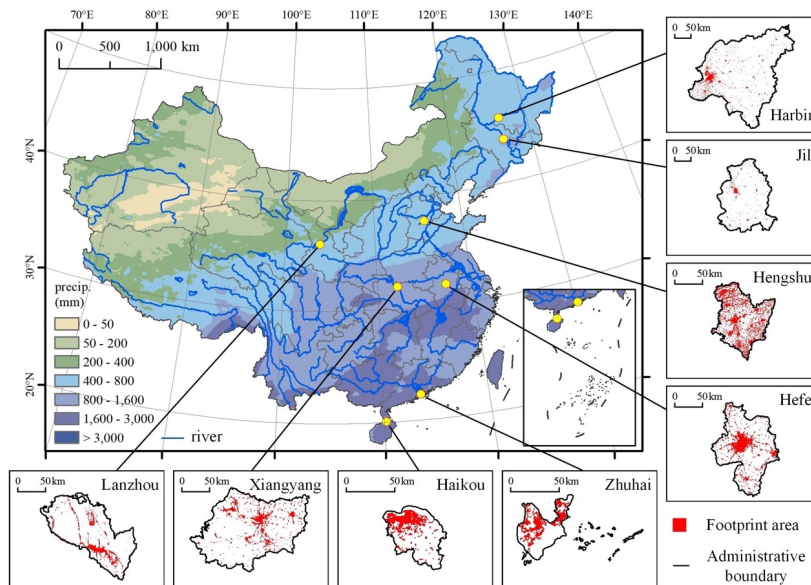
Figure 1 A map showing the geographic locations, annual precipitation, and footprints of the eight cities in this study.

Table 1 Statistics of the cities

Region	City	Population (10^4)	Footprint area (km^2)	Urbanization rate (%)
Southern China	Haikou	227.21	625	78.21
	Zhuhai	176.54	567	89.37
Central China	Hefei	796.50	1927	73.75
	Xiangyang	565.40	1817	59.65
Northern China	Lanzhou	372.96	1219	81.02
	Hengshui	446.04	2997	50.60
Northeastern China	Harbin	1092.90	2083	64.50
	Jilin	415.35	704	52.80

2.2 Data collection

The smartphone location data was obtained from the Tencent big data portal (https://heat.qq.com/). The portal provides location request records of the global smartphone users via the Tencent Map API. A location request record is generated when a smartphone user requests any LBS, which include but are not limited to navigation, car hailing, food and merchandise delivery, or social media check-ins. Table 2 lists part of the LBS applications that collect user's location requests. The portal releases the number of location requests per 0.01×0.01 regular grid for every 4-5 minutes. Comparing with other Chinese social media platforms, Tencent is the most popular one with the largest social community, which reported to have nearly 1.1 billion monthly active users for 2018 (https://www.tencent.com/en-us/company.html). Ma (2019) compared the NLR dataset with visitor numbers in a few places and confirmed that the NLR data is a good proxy for investigating dynamic population changes. We collected the NLR data of the grids within the administrative boundaries of the eight cities from August 1 to 31, 2017.

This study used the Version 05B GPM/IMERG 30-minute precipitation dataset (Huffman et al. 2018), which has a spatial resolution of 0.1×0.1 degrees. This dataset has been evaluated and widely used (Wang et al. 2017; Zhao et al. 2018; Su et al. 2018). The news reports about the flooding events in the eight cities were mainly collected from the Chinese mainstream online media, including Xinhuanet, Ecns.cn, Sohu, etc.

Table 2. Common smartphone applications using location-based services

Application	Type	LBS use case
WeChat	Mobile messaging app	Share location with friends
Mobile QQ	Mobile messaging app	Share location with friends
QQ Browser	Mobile web browser app	Push notifications of local news and weather
Qzone	Social network platform	Post geo-tagged microblogs

批注 [YJ1]: The revised part describing more about the Tencent location request data.

5

QQ Music	Mobile music app	Listen to music while running
Tencent Video	Mobile video app	Upload geo-tagged videos
Tencent News	Mobile news app	Push notifications of local news
JingDong (JOYBUY)	Mobile e-commerce platform	Location-based product recommendation
DiDi	Mobile transportation platform	Location-based car hailing
Meituan Waimai	Mobile on-demand delivery app	Location-based restaurant recommendation
Dianping	Mobile review and rating app	Location-based recommendation of restaurants, hotels, shops, etc.
Wangzhe Rongyao	Mobile game	Interact with nearby players

3 Methods

3.1 Time series anomaly detection

The smartphone location request record can be represented by a series of spatial points: $\{(x_i, y_i, Ts_i)\}$, $i=1,2,\ldots,n$. Each point contains its geographic coordinates (x, y) and a time (T) when the LBS is requested. The NLR was then aggregated to time series per grid or per city as illustrated below.

At the city level, a time series hourly NLR was established by adding up all location requests of the grids within the footprint area of that city. The magnitudes of the NLR in different cities vary significantly due to the different numbers of smart phone users. To make the NLR in different cities comparable, we normalized the NLR using the median-interquartile normalization method, which is more robust to

anomalies than other common approaches using sample mean and standard deviation (Geller et al. 2003).

We employed the S-H-ESD method (Vallis et al. 2014) to detect anomalies from the time series NLR, which can be represented by the following additive model

$$Ts=T+S+R \tag{1}$$

where *T, S,* and *R* denote the trend, seasonality and residual components in the time series data, respectively. The S-H-ESD method assumes that the trend and the seasonality would not be significantly disrupted by rapid-evolving events that last for only a few hours. Two major steps are involved in the method. First, it uses the piecewise median method to fit and remove the long-term trend and then the STL to remove seasonality (Cleveland et al. 1990). Using the STL to remove the long-term trend would introduce artificial anomalies (Vallis et al. 2014). In this study, the underlying trend in the time series NLR is approached using a piecewise combination of the biweekly medians, which show little changes over the whole time series.

In the second step, the S-H-ESD method employs the generalized Extreme Studentized Deviate (GESD) statistic (Rosner 1975) to identify the significant anomalies in the residuals. The GESD calculates the statistic (G) based on the mean ($\bar{r}$) and the standard deviation (s) of the observations:

$$G = \frac{max|r_j-\bar{r}|}{s} \tag{2}$$

Given the upper bound of *u* suspected anomalies, the GESD performs *u* separate tests. In each test, the GESD re-computes the statistic *G* after removing the observation r_j that maximizes $|r_j - \bar{r}|$ and then compares *G* with the critical value λ as defined below:

$$\lambda = \frac{(k-1)t_{1-a/(2k),k-2}}{\sqrt{k\left(k-2+t^2_{1-a/(2k),k-2}\right)}} \tag{3}$$

where *k* denotes the number of the observations in the time series after eliminating a suspected anomaly in the last run, and $t_{p,d}$ represents the pth percentile of a *t* distribution with a degree of freedom *d*. In this study, we set the significance level *a* as 0.05 and the number of anomalies no more than 25% of the total observations. Each test identifies one anomaly in the residuals when $G > \lambda$. The identified anomaly is either a positive or negative, depending upon whether the residual is greater or smaller than 0, respectively.

3.2 Anomaly measures and scores

In this study, an individual anomaly is represented with a vector,

$$v=(x, y, t, obs, res) \tag{4}$$

where x and y denote the coordinates of the grid centroid, t denotes the observation time, obs and res denote the observation and the residual (R in equation 1) in the time series. This study uses an anomaly's absolute residual to describe its unusual deviation from its expectation.

A rainstorm disaster, once significantly impacts the cities, usually can trigger an outbreak of NLR anomalies in multiple places across the city. To collectively characterize the abnormal human responses, this study defines three indices: the total number (N_t), the total residual (R_t), and the mean density (D_t) of the positive or negative anomalies. The mean density is defined as follows:

$$D_t = \frac{\sum_{i=1}^{N_t} B_i}{N_t} \tag{5}$$

where B_i denotes the number of neighborhood anomalies within a Manhattan distance of a 5-grid (~5 km) radius of the ith anomaly. The radius is large enough to cover most urban facilities nearby the anomaly.

An anomaly score is then defined based on the afore-mentioned indices to evaluate the city residents' responses to a rainstorm event. First, we surveyed the hourly changes of the indices and calculated the quartiles (Q_1, Q_2, Q_3) and interquartile range (IQR) of each index for every hour every day. The score of an index is defined by:

$$S_{V,t} = \begin{cases} \frac{V_t - Q_1}{IQR} & , if\ V_t \leq Q_1 \\ 0 & , if\ Q_1 < V_t < Q_3 \\ \frac{V_t - Q_3}{IQR} & , if\ V_t \geq Q_3 \end{cases} \tag{6}$$

where V_t represents one of the three indices at time t. According to Tukey's fences (Tukey 1977), the score is considered an outlier if its absolute value is greater than 1.5 or an extreme if it is greater than 3. The final anomaly score is the mean of the three index scores.

3.3 Characterization of a rainfall event

In this study, we examined the city residents' responses to the rainfall events in August 2017. The national average precipitation of this month is 124.6 mm, which is the highest in 2017 and 21.3% more than the August average precipitation in previous years.

We defined a rainfall event as a precipitation process that lasts for at least two hours and with no rain preceding it for at least one hour. The severity of a rainfall

8

event is described by its duration, accumulated precipitation, and peak rainfall
intensity. The duration refers to how long a rainfall event lasts, and the accumulated
precipitation is the total precipitation received during a rainfall event. The peak
rainfall intensity (I_d) is widely used to estimate the possible rainfall intensity
threshold that triggers city (Cannon et al. 2007; Diakakis 2012) and is defined as
below:

$$I_d = \frac{\max\{\sum_{i=j}^{j+d-1} P_i\}}{d}, \quad j = 1, 2, \ldots, N-d+1 \quad (7)$$

where P_i denotes the precipitation during the ith time interval, N denotes the total
number of the time intervals in a rainfall time series, and d denotes the width of the
moving time window that was used to search for the maximum accumulated
precipitation in a rainfall event. Based on the peak rainfall intensity, the August
rainfall events in the eight cities can be categorized into moderate rainstorm (0.5
mm/h < I_1 ≤ 4 mm/h), heavy rainstorm (4 mm/h < I_1 ≤ 8 mm/h), and violent rainstorm
(I_1 ≥ 8 mm/h).

For calculation purpose, we downscaled the precipitation data to the same
spatial resolution as that of the NLR using the nearest-neighbor interpolation method.
At the city level, the rainfall of a city is defined as the total of the half-hour TRMM
precipitation within the human footprint. At the grid level, the rainfall of each grid
refers to the total precipitation received by that grid within a certain time period.

4 Results

**4.1 Rainfall characteristics and peak rainfall intensity thresholds**

The eight cities could be categorized into two groups in terms of the total
precipitation amount in August 2017 (Fig. 2a). The first group includes Haikou, Zhuhai,
and Hefei, with total precipitation more than 400 mm. The summer monsoon brings
plenty of water to the two coastal cities (i.e. Haikou and Zhuhai). The Typhoon Hato,
when it made landfall on August 23, further dumped 68- and 108-mm water to
Hiakou and Zhuhai, respectively. By contrast, the inland city Hefei, received 47.6%
more precipitation in 2017 than the average mainly due to a few unusual rainstorms
in August 2017 (Hydrology and Water Resource Bureau of Hefei 2018)

The second group includes all the other cities, which have less than 400 mm
precipitation in August 2017. The city Lanzhou is located in the dry northwestern
China and has the least precipitation of 250 mm. The two inland cities, Xiangyang
and Hengshui both have slightly higher precipitation of 300 mm. The precipitation of
the two northeastern cities, Harbin and Jilin, ranges between 320 and 350 mm and is
mainly brought in by the northwestern vortexes.

There are at least 15 rainstorms and two flooding events in each city. The city

Haikou, Lanzhou, and Harbin witnessed more than 20 rainstorms and about 1/4 out of them caused serious flooding problems. The number of rainstorms in the other cities ranges from 15 to 20 and about two to four out of them caused flooding problems in the cities.

We identified the peak rainfall intensity threshold value that likely triggers city flooding using the method developed by Cannon et al. (2008) and Diakakis (2012). The method plots peak rainfall intensity of different time windows against the corresponding rainfall duration. The flood-triggering threshold is defined as the upper limit of the peak rainfall intensity that tends to lead to urban flooding but actually not. As shown in Fig. 2b, for the rainfall thresholds calculated based on 0.5-, 1-, 2-, and 3-hour time window, the city ranking shows no change with an order of Haikou, Jilin, Hengshui, Zhuhai, Hefei, Lanzhou, Harbin, and Xiangyang. The ranking shows some fluctuations when the flooding-triggering rainfall threshold values were calculated with a more than 3-hour time window. However, Haikou and Harbin are always the top two cities whereas Xiangyang is the last one on the ranking list. It is worthy to note that a rainstorm with a peak rainfall intensity over the threshold 5 mm/h would definitely trigger floods in Xiangyang. However, in Haikou, such a threshold value is 30 mm/h. In other words, city flooding would occur in Haikou when it is hit by a rainstorm with peak rainfall intensity over 30mm/h. In general, the difference between the threshold values among these cities reduces with a longer time window, indicating that the rainfall in a shorter time window is more critical to evaluate whether a city is prone to flooding.
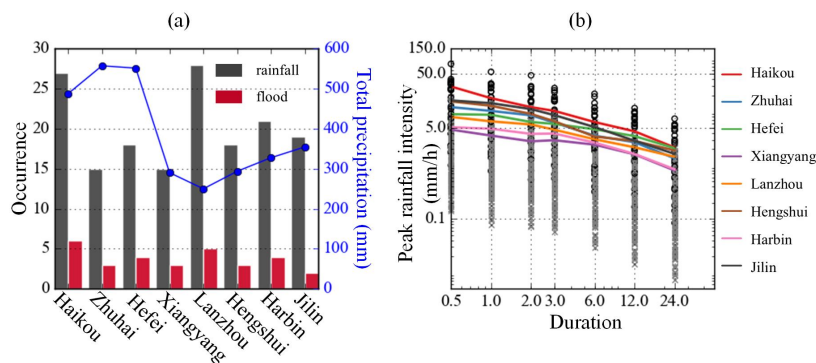
Figure 2. Total August precipitation and frequency of rainfall and city flooding events (a). Variations in peak rainfall intensity (circles) and the flooding-triggering precipitation threshold values (lines) that are derived from time windows ranging from 0.5 to 24 hours (b).

4.2 Normal rhythm of city

The NLR records can serve as a proxy of the city residents' normal daily routine. The normalized NLR show the eight cities have a similar diurnal rhythm (Fig. 3a). The normalized NLR median climbs from a minimum at around 4:00 and to a peak right at 12:00. It starts to drop slightly and then peaks again at around 20:00. This general pattern reflects the smartphone usage patterns of the city residents. Phone usage starts to drop after the midnight when most residents start to rest. It reaches its first peak during the lunch time as residents may request more LBS to find a place to eat. After lunch time, phone usage remains at a high plateau, probably due to more LBS requests for business purposes. Phone usage reaches the highest peak of the whole day right after the normal work hours, indicating a significant increased need for the LBS such as hailing nearby taxis to socialize with friends, go back home, or sending geo-tagged posts for socializing.

The general diurnal pattern was superposed with subtle short-term NLR variations. The NLR in the southern cities peaks and hits the bottom later at night and before dawn, respectively, than that of the northern cities. This is very likely due to the different lifestyles between the northern and southern residents in response to the economic activities and day length. It is well-known that the southern China is more active in economic and social activities and the southerners enjoy the night activities more (Ma et al. 2019). By contrast, the northerners tend to end their nightlife earlier and also become active earlier as the day breaks earlier in the north.

The total NLR is moderately correlated with the population of these cities (Fig. 3b). The 0.63 Pearson correlation coefficient (with a *p* value of 0.046) indicates a statistically significant positive relationship between the normalized NLR and the population. As a result, we believe the NLR data could reflect the collective geo-tagged behaviors of the city residents as a whole and consequently it could serve as a proxy of the human responses to different environmental and social events.
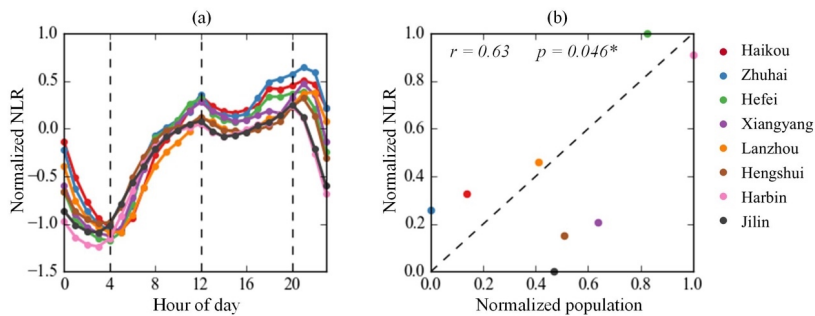
Figure 3. The diurnal variation patterns of the NLR in the eight cities (a) and a positive correlation between the NLR and the total number of residents (b).

4.3 Urban anomalies during rainstorms

4.3.1 City-scale analysis

There are more positive than negative anomalies in the August time series hourly NLR and most positive anomalies were found in pair with precipitation spikes (Fig. 4). For example, two significant precipitation spikes in Harbin in the afternoon of August 2nd and 3rd were closely associated with positive NLR anomalies. Few NLR negative anomalies were identified in the eight cities except Zhuhai. This city was significantly affected by Typhoon Hato, which brings huge amount of precipitation and leads to a negative anomaly since the Afternoon of August 23rd in Zhuhai. Such a significant negative anomaly could be attributed to serious communication interruption or damages caused by the typhoon.

It is worthy to note that both positive and negative anomalies were also identified when there is no rain in the cities. For example, two positive anomalies were identified around August 28th in Harbin when there is no rain at all. The no-rain anomalies must be triggered by other major events in the cities. However, at this moment it is not easy to trace what local events may trigger such anomalies.

It is very interesting to notice that a couple of no-rain positive anomalies were identified in the last week of August for almost all eight selected cities except Zhuhai. These positive anomalies were obviously not associated with any special rainstorm events. Instead, they are more likely to be associated with sort of national-wide events, such as the college students' back to school and move-in events, which are mainly scheduled in the last week of August every year in China. Such positive anomalies were not found in Zhuhai, of which the 2017 back to school and move-in events was postponed to the first week of October due to the significant damages caused by Typhoon Hato. However, further studies, such as of the NLR of other cities in China, are needed to consolidate this argument.
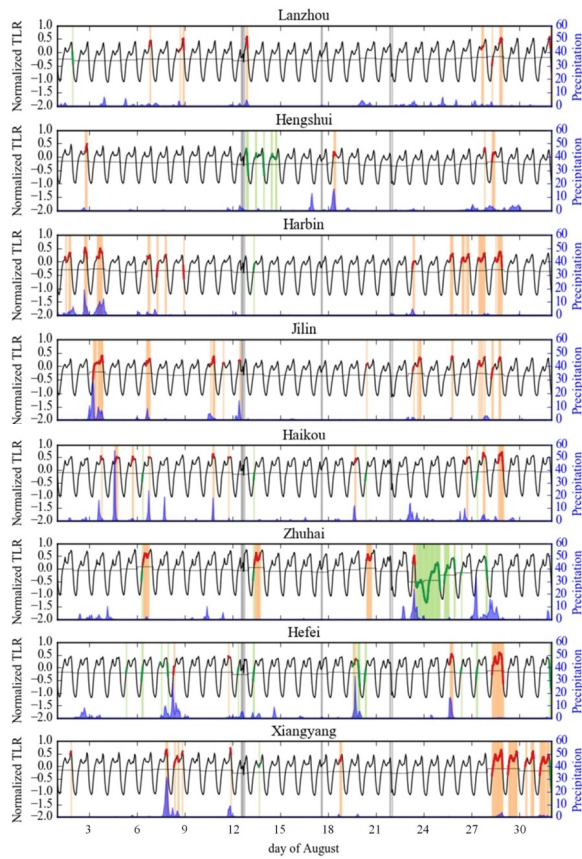
1

2 Figure 4. The time series NLR and rain events during August 2017. Positive and

3 negative anomalies were shown in orange and green colors, respectively. The light

4 gray columns show the periods when NLR data is missing.

5

6   We further quantitatively examined the association between rainfall events and

7 the NLR anomalies. Table 3 lists the R_{pos} and R_{neg}, which are the ratios of the positive

8 and negative anomalies corresponding to the four scenarios (no rains, moderate,

9 heavy and violent rainstorm events) to the total number of anomalies identified over

10 the whole time series, respectively. As shown in Table 3, in total we identified 27, 19,

11 78, and 166 violent, heavy, moderate, and no rainstorm events in the eight cities,

12 respectively. Under different scenarios, the R_{pos} is always higher than R_{neg} except the

13 no rain scenario, in which there is no significant difference between these two ratios.

14 The rainstorm-related R_{pos} increases from 0.22 to 0.70 as the rainstorms level up

15 from moderate to violent as compared to a no-rain R_{pos} of 0.12. The rain-related or

13

no-rain R_{neg} is no more than 0.22. The R_{pos} is much higher than R_{neg} when the cities are affected by stronger rainfall events. For example, when the cities are affected by violent storms, the R_{pos} and R_{neg} are 0.70 and 0.22 respectively. By contrast, the R_{pos} and R_{neg} are 0.22 and 0.06, respectively when the cities are affected by moderate rainstorms. It is very likely that, when there are severe rainstorms, people may send out more LBS requests in order to, for instance, search a route free of inundation spots and less congested roads, order delivery food, or post geo-tagged photos of the terrible moments.

A lower R_{pos} of the heavy and moderate rainstorms may also be partly attributed to the effect of data aggregation at the city scale. It is very common that a rainstorm may influence only a part of the city and only lead to certain local positive anomalies. In such a case, increase of the NLR in a small number of grids may not result in significant changes of the NLR of the entire city and consequently no anomalies at the city level. Analysis at the grid level, as reported in the next section, would show how residents respond to the local rainstorm events.

The difference between the R_{pos} and R_{neg} also varies for different cities. For example, the two violent rainstorms both trigger a positive anomaly in Xiangyang and Harbin. By contrast, the five violent rainstorms in Zhuhai lead to the same percent positive and negative anomalies. City Hefei is special. The same percent of positive and negative anomalies are triggered by the five violent storms. However, when Hefei is affected by the moderate and heavy rainstorms or even no rainfalls, there are slightly more negative than positive anomalies.

Table 3. Numbers of different categories of rainstorms and the corresponding R_{pos} and R_{neg}.

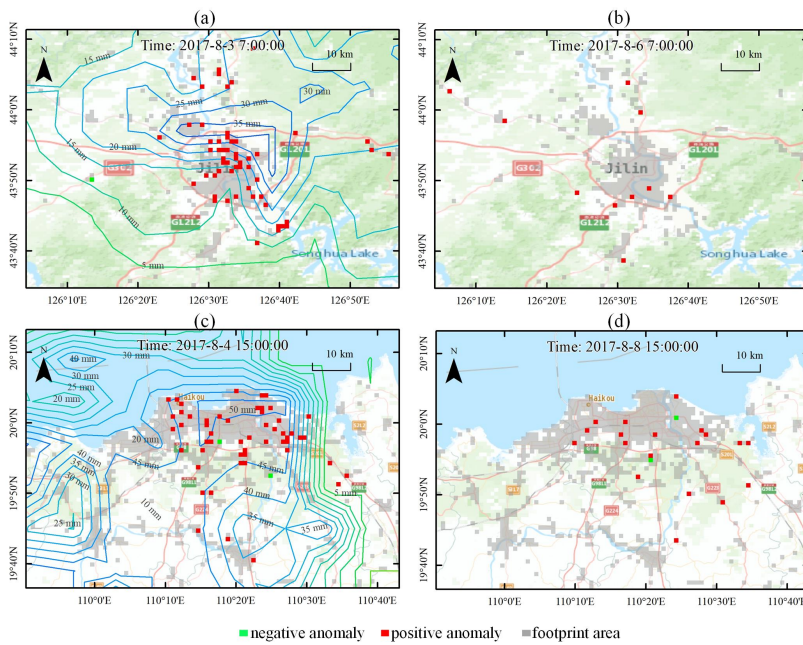| Cities	No rainfall			Rainstorms								
				Moderate			Heavy			Violent		
	N	R_{pos}	R_{neg}	N	R_{pos}	R_{neg}	N	R_{pos}	R_{neg}	N	R_{pos}	R_{neg}
Haikou	27	0.04	0.22	14	0.21	0.00	3	0.33	0.00	8	0.75	0.00
Zhuhai	16	0.19	0.25	5	0.20	0.20	3	0.00	0.00	5	0.40	0.40
Hefei	19	0.05	0.32	7	0.00	0.14	2	0.50	1.00	5	0.60	0.60
Xiangyang	15	0.33	0.33	7	0.29	0.00	0	-	-	2	1.00	0.00
Lanzhou	29	0.07	0.10	17	0.24	0.06	5	0.20	0.20	0	-	-
Hengshui	19	0.00	0.21	11	0.18	0.09	2	0.00	0.00	2	0.50	0.00
Harbin	21	0.24	0.10	7	0.14	0.14	3	1.00	0.00	2	1.00	0.00
Jilin	20	0.15	0.15	10	0.40	0.00	1	1.00	0.00	3	1.00	0.33
Overall	166	0.12	0.20	78	0.22	0.06	19	0.37	0.11	27	0.70	0.22

4.3.2 Grid-scale analysis: anomaly indices

The S-H-ESD method was also used to detect the NLR anomalies at the grid level. There are always more grids showing anomaly when the city was affected by a

14

1   rainstorm. Figure 5 provides an example to illustrate the grids with anomaly detected

2   during a rainstorm and the same time period in another day without rainfall in Jilin

3   and Haikou, respectively. Anomalies were identified in 56 grids in Jilin when it was hit

4   by a rainstorm at 7am on August 3, 2017. By contrast, anomalies are observed in only

5   10 grids during the same time period on August 6, 2017 when there is no rain at all.

6   In Haikou, anomalies are found in 52 grids during a rainstorm and only 19 grids when

7   there is no rain.

8

Figure 5. Grid with negative and positive anomalies within the footprint areas of Haikou and Jilin. The contour lines show the precipitation.

9   Figure 5. Grid with negative and positive anomalies within the footprint areas of

10   Haikou and Jilin. The contour lines show the precipitation.

11

12   The total number, total residual, and mean density of these anomalies were

13   then calculated (Fig. 6) for the cities when they were affected by flooding caused by a

14   typical rainstorm event (Table 4). The three anomaly indices show similar diurnal

15   variations as of the NLR diurnal rhythm and they all spiked to the level of an outlier

16   or even to an extreme value when the city was significantly affected by flooding

15

1 issues.

2   After the spikes, the anomaly indices usually bounce back to the same level

3 before for almost all the cities except Zhuhai, indicating most cities return to their

4 normal rhythms after the rainstorm interruption. However, Zhuhai was hit by the

5 category-3 Typhoon Hato at around 12:50 on August 23. The typhoon brought

6 intense rain, strong winds, and caused significant flooding issues and damages to the

7 city infrastructures, causing a sharp decline and persistent negative anomalies after

8 the landfall of Hato. It took more than 72 hours for the anomaly indices to bounce

9 back to the same level before Hato (not shown in Fig. 6).

10

11 Table 4. An exemplary flooding event in each of the cities.

12

City	Urban flood event	Rainfall duration (h)	Accumulated precipitation (mm)	Half-hour peak rainfall intensity (mm/h)
Haikou	8-4 15:00	10	117	77
Zhuhai	8-23 12:50	23	108	32
Hefei	8-25 17:00	13	72	25
Xiangyang	8-7 18:00	30.5	140	34
Lanzhou	8-12 21:00	9.5	14	5
Hengshui	8-18 08:00	15	67	18
Harbin	8-2 17:00	12.5	61	26
Jilin	8-3 07:00	38.5	185	31

13
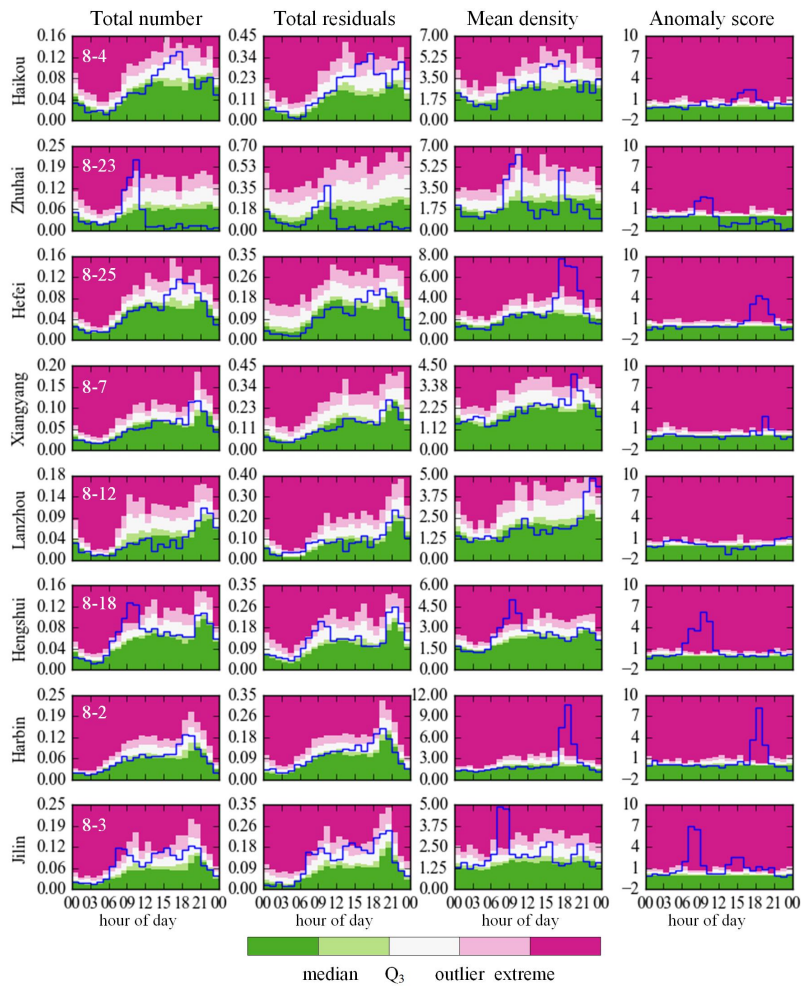
Figure 6. Intra-day variations in NLR, total residuals, mean density, and anomaly score within 24 hours of a typical flooding event in each of the cities.

4.3.3 Grid-scale analysis: anomaly score and rainfall intensity

Given the anomaly score is indicative of the unusual responses of residents to rainstorms, we further examined the relation between the anomaly score and the rainfalls in these cities during the August 2017.

17

The grid-level R_{pos} is much higher than the city-level counterpart with respect to all types of events (Fig. 7a). Such a difference is mainly due to the different analysis levels. We can easily identify the local anomalies per grid, which are more likely to be obliterated at the city level due to the data aggregation. At the grid level, the R_{pos} and R_{neg} also vary in response to the different levels of rainstorm events. All cities show a higher R_{pos} when they are affected by violent rainstorms (85%) than heavy rainstorms (68%), in comparison with the R_{pos} (56%) when the cities are not affected by any rainfall events. However, the R_{pos} of moderate rainstorms (45%) is less than the no-rain R_{pos}, likely suggesting that low-intensity rainfall events may not necessarily trigger NLR anomalies and other factors may contribute to the NLR anomalies at the grid level.

How easily the rhythm of a city would be disrupted by a rainstorm is strongly related to the anomaly-triggering peak rainfall intensity threshold (Fig. 7b), which was calculated using the same the ideas in the methods developed by Cannon et al. (2008) and Diakakis (2012). We plotted the peak rainfall intensity with respect to whether there are anomalies or not for each city. The anomaly-triggering peak rainfall intensity is defined as the upper limit of the rainfall intensity that tends to lead to an NLR anomaly but actually not.

Every rainstorm with its peak intensity higher than the threshold would definitely trigger an NLR anomaly. As a result, the cities with a lower threshold tend to be more easily disrupted by a moderate or heavy rainstorm. For example, Xiangyang has a very low threshold value of 1.4 mm/h. In August 2017, there are six rainstorm events with peak rainfall intensity exceeding this threshold and they all caused anomalies in this city.

However, even a rainstorm with its peak rainfall intensity below the threshold may also trigger an NLR anomaly. For example, quite a few NLR anomalies were found in Lanzhou, of which most rainstorms have its peak rainfall intensity below the threshold (6.6 mm/h). This is because a heavy rainstorm at around 24:00 failed to trigger an NLR anomaly as most people were sheltered at home and hence were not affected. However, this rainstorm is included in the process to calculate the peak

rainfall intensity and increase the threshold. As a result, rainstorms with their peak rainfall intensity below the threshold may also trigger anomalies, particularly in the cities with more heavy and violent rainstorms after late night and before dawn.

The anomaly score is correlated with rainfall intensity for some cities (Fig. 7c). Specifically, there are three cities, i.e. Harbin, Jilin, and Haikou, showing a positive linear relationship between the anomaly score and rainfall intensity. The p-values in the linear regression analysis are less than 0.05, suggesting the correlations are statistically significant. As the rainfall intensity increases, the anomaly scores of the three cities increase linearly. Furthermore, the slope coefficients of the correlations indicate how sensitive the rainfall intensity may trigger anomalies. The city Harbin has the steepest slope thus slightly increase in rainfall intensity would trigger anomalies more easily. By contrast, the gentlest slope indicates Haikou is a city where the residents, in terms of their LBS request, are not very sensitive to the increase of the rainfall intensity. Such diverse sensitivity may be essentially due to different climatic conditions, infrastructure levels or other potential factors in these cities. The city Haikou is situated in humid climate zone with average rainfall exceeding 1600 mm per year, greater than the other two cities. Meanwhile, considering the drainpipe density, which is defined as the ratio of the total length of drainpipes to the built-up area of a city, we found Haikou also has higher drainpipe density (11.74 km^{-1}) than the rest two cities (5.73 km^{-1} for Jilin and 7.44 km^{-1} for Haikou)[1]. So, although rainstorms frequently hit Haikou, their impacts on local residents could be much lessened by efficient drainage system.

Around 31%, 23%, and 46% of the maximum anomaly scores were detected before, at the same time, and after the rainfall intensity reaches its peak (Fig. 7d). Specifically, 23%, 24%, and 20% of the anomaly score peaks simultaneously, within 1 hour, and within 2 hours of the rainfall intensity peaks, respectively. About 46% of the anomaly score peaks after the rainfall intensity peaks, which is 50% more than the number of the cases that anomaly score peaks ahead of the rainfall intensity

批注 [YJ2]：The revised part describing the significant correlation between peak rainfall intensity and anomaly score in three cities.

批注 [YJ3]：The revised part discussing the factors that may lead to the different sensitivity to rainstorms among the cities.

---

[1] The data are from the 2017 year book of the cities available at http://tongji.cnki.net/kns55/Navi/NaviDefault.aspx.

peak. As a result, we usually see the maximum positive anomalies (i.e. significant

disturbance in city rhythm) after the rainfall intensity reached a maximum value. It is

also possible for the anomaly to reach its peak before the peak of the rainfall

intensity if, for example, the cumulative rainfall is high enough to significantly impact

the city.
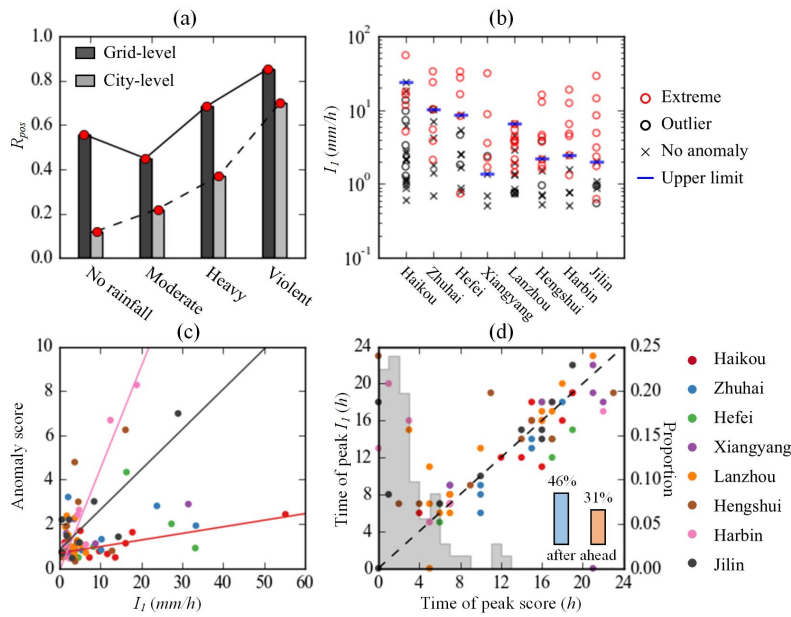
Figure 7. Correlation between peak rainfall intensity and anomaly score.

5. Conclusions

This study shows the potentials of the NLR data in reflecting city residents'

collective geo-tagged behaviors. First of all, the NLR was moderately correlated with

the population of the cities. Secondly, the time series NLR data well corresponds to

the regular diurnal rhythm in all eight cities, which is characterized by limited

activities from the midnight to early morning and very active LBS requests from noon

to the evening. Thirdly, the time series NLR also reflects the different lifestyles in the

northern and southern China, showing southerners enjoy late night life more

whereas the northerners start their days earlier in the morning.

The anomalies of the NLR data are well with that the rainstorms, especially the violent ones, were very likely to trigger positive NLR anomalies at city level. At the grid level, the anomalies in response to rainstorms show a significant increase in the anomaly indices in terms of the total number, total residual, and mean density. The time series composite score derived from these three anomaly indices clearly shows how city residents respond to rainstorms in terms of their LBS requests.

Rainstorms of the same magnitude may not trigger NLR anomalies in the same way in every city. Essentially, the peak rainfall intensity of the rainstorms seems to be the key and such a threshold is significantly different among different cities. As a result, high peak rainfall intensity tends to trigger flooding and subsequently anomalies in the NLR data. Furthermore, the peak rainfall intensity is well associated with the peak anomaly score, further indicating it is the key factor that can trigger rainstorm-induced NLR anomalies.

It is worthy to note that other events may also contribute to NLR anomalies. There are a couple of positive anomalies in the last week of August for almost all cities except Zhuhai. The last week of August is the school registration time for college students in China. It is reasonable to expect such a nation-wide event may trigger NLR anomalies as shown in this study. However, some college cities may postpone the registration time and Zhuhai is one of them due to the significant damages caused by Typhoon Hato right before the registration week.

We are also aware of limitation of the Tencent location request dataset. Although the dataset is generated by more than one billion monthly active users, it still cannot fully represent the entire population of a city. The collective response analysis based on the location requests consequently may underestimate rainstorm impacts upon infrequent users, particular the older and children. Future studies will combine multi-source geospatial datasets to address the limitation and further explore human responses to various weather events.

批注 [YJ4]：The revised part discussing the limitation of the Tencent location request data and future plans to address it.

Data availability

The IMERG data were from the NASA/Goddard Space Flight Center's PMM and PPS, available at http://pmm.nasa.gov/data-access/downloads/gpm (accessed 14 April 2019). Other analyzed datasets and generated results in the study are available from the corresponding author on reasonable request.

Author contribution

YD and CZ developed the framework of the study. TP and TM collected the data and designed the experiment. JY performed the data analysis. JY and FL prepared the manuscript and revision.

Competing interests

The authors declare that they have no conflict of interest.

References

Adelekan, I. O.: Vulnerability assessment of an urban flood in Nigeria: Abeokuta flood 2007, Nat. Hazards, 56(1), 215–231, doi:10.1007/s11069-010-9564-z, 2011.

Alexander, L. V., Zhang, X., Peterson, T. C., Caesar, J., Gleason, B., Klein Tank, A. M. G., Haylock, M., Collins, D., Trewin, B., Rahimzadeh, F., Tagipour, A., Rupa Kumar, K., Revadekar, J., Griffiths, G., Vincent, L., Stephenson, D. B., Burn, J., Aguilar, E., Brunet, M., Taylor, M., New, M., Zhai, P., Rusticucci, M. and Vazquez-Aguirre, J. L.: Global observed changes in daily climate extremes of temperature and precipitation, J. Geophys. Res. Atmos., 111(5), 1–22, doi:10.1029/2005JD006290, 2006.

Bagrow, J. P., Wang, D. and Barabási, A.-L.: Collective Response of Human Populations to Large- Scale Emergencies, PLoS One, 6(3), 1–8, doi:10.1371/journal.pone.0017680, 2011.

Barberia, L., Amaro, J., Aran, M. and Llasat, M. C.: The role of different factors related to social impact of heavy rain events : considerations about the intensity thresholds in densely populated areas, Nat. Hazards Earth Syst. Sci., 14, 1843–1852, doi:10.5194/nhess-14-1843-2014, 2014.

Cannon, S. H., Gartner, J. E., Wilson, R. C., Bowers, J. C. and Laber, J. L.: Storm rainfall conditions for floods and debris flows from recently burned areas in southwestern Colorado and southern California, Geomorphology, 96(3–4), 250–269, doi:10.1016/j.geomorph.2007.03.019, 2007.

China National Climate Center: Bulletin of Flood and Drought Disaster in China 2017, 2017.

Cleveland, R. B., Cleveland, W. S., MaRae, J. E. and Terpenning, I.: STL: A Seasonal-Trend Decomposition Procedure Based on Loess, J. Off. Stat., 6(1), 3–73, 1990.

Diakakis, M.: Rainfall thresholds for flood triggering. The case of Marathonas in Greece, Nat. Hazards, 60(3), 789–800, doi:10.1007/s11069-011-9904-7, 2012.

Dobra, A., Williams, N. E. and Eagle, N.: Spatiotemporal detection of unusual human population behavior using mobile phone data, PLoS One, 10(3), e0120449, doi:10.1371/journal.pone.0120449, 2015.

Geller, S. C., Gregg, J. P., Hagerman, P. and Rocke, D. M.: Transformation and normalization of oligonucleotide microarray data, Bioinformatics, doi:10.1093/bioinformatics/btg245, 2003.

Goodchild, M. F. and Glennon, J. A.: Crowdsourcing geographic information for disaster response : a research frontier, Int. J. Digit. Earth, 3(3), 231–241, doi:10.1080/17538941003759255, 2010.

Gundogdu, D., Incel, O. D., Salah, A. A. and Lepri, B.: Countrywide arrhythmia: emergency event detection using mobile phone data, EPJ Data Sci., 5(1), doi:10.1140/epjds/s13688-016-0086-0, 2016.

Hu, P., Zhang, Q., Shi, P., Chen, B. and Fang, J.: Flood-induced mortality across the globe: Spatiotemporal pattern and influencing factors, Sci. Total Environ., 643, 171–182, doi:10.1016/j.scitotenv.2018.06.197, 2018.

Hydrology and Water Resource Bureau of Hefei: Bulletin of Flood and Drought Disaster in Hefei, 2018.

Kryvasheyeu, Y., Chen, H., Obradovich, N., Moro, E., Van Hentenryck, P., Fowler, J. and Cebrian, M.: Rapid assessment of disaster damage using social media activity, Sci. Adv., 2(3), e1500779, doi:10.1126/sciadv.1500779, 2016.

Kubal, C., Haase, D., Meyer, V. and Scheuer, S.: Integrated urban flood risk assessment – adapting a multicriteria approach to a city, Nat. Hazards Earth Syst. Sci., 9, 1881–1895, doi:10.5194/nhess-9-1881-2009, 2009.

Liao, X., Xu, W., Zhang, J., Li, Y. and Tian, Y.: Global exposure to rainstorms and the contribution rates of climate change and population change, Sci. Total Environ., 663, 644–653, doi:10.1016/j.scitotenv.2019.01.290, 2019.

Llasat, M. C., Llasat-Botija, M., Barnolas, M., Ĺopez, L. and Altava-Ortiz, V.: An analysis of the evolution of hydrometeorological extremes in newspapers: The case of Catalonia, 1982-2006, Nat. Hazards Earth Syst. Sci., 9(4), 1201–1212, doi:10.5194/nhess-9-1201-2009, 2009.

Ma, T.: Quantitative responses of satellite-derived night-time light signals to urban depopulation during Chinese New Year, Remote Sens. Lett., 10(2), 139–148, doi:10.1080/2150704X.2018.1530484, 2019.

Ma, T., Pei, T., Song, C., Liu, Y., Du, Y. and Liao, X.: Understanding geographical patterns of a city's diurnal rhythm from aggregate data of location-aware services, Trans. GIS, doi:10.1111/tgis.12508, 2019.

Miao, Q., Yang, D., Yang, H. and Li, Z.: Establishing a rainfall threshold for flash flood warnings in China's mountainous areas based on a distributed hydrological model, J. Hydrol., 541, 371–386, doi:10.1016/j.jhydrol.2016.04.054, 2016.

Min, S. K., Zhang, X., Zwiers, F. W. and Hegerl, G. C.: Human contribution to more-intense precipitation extremes, Nature, 470(7334), 378–381, doi:10.1038/nature09763, 2011.

Papagiannaki, K., Lagouvardos, K. and Kotroni, V.: A database of high-impact weather events in Greece: A descriptive impact analysis for the period 2001-2011, Nat. Hazards Earth Syst. Sci., 13(3), 727–736, doi:10.5194/nhess-13-727-2013, 2013.

Papagiannaki, K., Lagouvardos, K., Kotroni, V. and Bezes, A.: Flash flood occurrence and relation to the rainfall hazard in a highly urbanized area, Nat. Hazards Earth Syst. Sci., 15(8), 1859–1871, doi:10.5194/nhess-15-1859-2015, 2015.

Papagiannaki, K., Kotroni, V., Lagouvardos, K., Ruin, I. and Bezes, A.: Urban Area Response to Flash Flood–Triggering Rainfall, Featuring Human Behavioral Factors: The Case of 22 October 2015 in Attica, Greece, Weather. Clim. Soc., 9(3), 621–638, doi:10.1175/wcas-d-16-0068.1, 2017.

Ratti, C., Frenchman, D., Pulselli, R. M. and Williams, S.: Mobile landscapes: Using location data from cell phones for urban analysis, Environ. Plan. B Plan. Des., 33(5), 727–748, doi:10.1068/b32047, 2006.

Rosner, B.: On the detection of many outliers, Technometrics, 17(2), 221–227, 1975.

Ruin, I., Creutin, J. D., Anquetin, S. and Lutoff, C.: Human exposure to flash floods - Relation between flood parameters and human vulnerability during a storm of September 2002 in Southern France, J. Hydrol., 361(1–2), 199–213,

doi:10.1016/j.jhydrol.2008.07.044, 2008.

Ruin, I., Lutoff, C., Boudevillain, B., Creutin, J.-D., Anquetin, S., Rojo, M. B., Boissier, L., Bonnifait, L., Borga, M., Colbeau-Justin, L., Creton-Cazanave, L., Delrieu, G., Douvinet, J., Gaume, E., Gruntfest, E., Naulin, J.-P., Payrastre, O. and Vannier, O.: Social and Hydrological Responses to Extreme Precipitations : An Interdisciplinary Strategy for Postflood Investigation, Weather. Clim. Soc., 6, 135–153, doi:10.1175/WCAS-D-13-00009.1, 2014.

Spitalar, M., Gourley, J. J., Lutoff, C., Kirstetter, P. E., Brilly, M. and Carr, N.: Analysis of flash flood parameters and human impacts in the US from 2006 to 2012, J. Hydrol., 519(PA), 863–870, doi:10.1016/j.jhydrol.2014.07.004, 2014.

Taylor, H. L., Webber, D., Becker, J. S., Gruntfest, E., Wright, K. C. and Doody, B. J.: A Review of People's Behavior in and around Floodwater, Weather. Clim. Soc., 7(4), 321–332, doi:10.1175/wcas-d-14-00030.1, 2015.

Terti, G., Ruin, I., Anquetin, S. and Gourley, J. J.: Dynamic vulnerability factors for impact-based flash flood prediction, Nat. Hazards, 79(3), 1481–1497, doi:10.1007/s11069-015-1910-8, 2015.

Tukey, J. W.: Exploratory Data Analysis, Addison-Wesley Publishing Company., 1977.

UNISDR: Sendai Framework for Disaster Risk Reduction 2015-2030., 2015.

Vallis, O., Hochenbaum, J. and Kejariwal, A.: A Novel Technique for Long-term Anomaly Detection in the Cloud, Proccedings 6th USENIX Work. Hot Top. Cloud Comput. (USENIX '14), 1–6, doi:10.1016/j.pupt.2014.03.006, 2014.

Wang, Q. and Taylor, J. E.: Quantifying human mobility perturbation and resilience in hurricane sandy, PLoS One, 9(11), 1–5, doi:10.1371/journal.pone.0112608, 2014.

Zhou, Y., Shen, D., Huang, N., Guo, Y., Zhang, T. and Zhang, Y.: Urban flood risk assessment using storm characteristic parameters sensitive to catchment-specific drainage system, Sci. Total Environ., 659, 1362–1369, doi:10.1016/j.scitotenv.2019.01.004, 2019.